Hindawi
Advances in Mathematical Physics
Volume 2024, Article ID 3931231, 15 pages
https://doi.org/10.1155/2024/3931231

Research Article

Transient Response of Multiple Interface Cracks in Fine-Grained Coating Composite Structures under Impact Loading

Shuaishuai Hu[1] **and Junlin Li**[2]

[1]*School of Mathematics and Statistics, Zhoukou Normal University, Zhoukou 466001, China*
[2]*School of Applied Science, Taiyuan University of Science and Technology, Taiyuan 030024, China*

Correspondence should be addressed to Shuaishuai Hu; hsshuai@163.com

Received 1 November 2023; Revised 27 January 2024; Accepted 28 March 2024; Published 17 April 2024

Academic Editor: Manuel De León

The mechanical behavior of the fine-grained piezoelectric/substrate structure with multiple interface cracks under the electromechanical impact loading is investigated. Using the Laplace and Fourier integral transforms, the double-coupled singular integral equations and single-valued conditions of the problems are formulated. Both the singular integral equation and single-valued conditions are simplified into an algebraic equation through the Chebyshev point placement method and solved by numerical calculation. Then, the expression of the dynamic energy release rate is given with the help of the dynamic intensity factors of electric displacement and stress obtained. Finally, numerical results of the dynamic energy release rate with material parameters are demonstrated. The results show that the dynamic energy release rate depends on the size of the interface cracks, coating thickness, and the mechanical–electrical loading. Meanwhile, the fine-grained piezoelectric structures exhibit safer structural performance compared to normal one.

1. Introduction

It is well-known that piezoelectric materials have played an important role in the manufacturing of intelligent system components due to their unique performance, such as sensors, actuators, and transducers. However, due to manufacturing processes and piezoelectric composite structures, various defects and damages often occur at the interface during the manufacturing process or under load conditions. When these defects and damages further expand, they could lead to overall structural failure. Compared to static loads, a deep understanding of the fracture criteria for interface cracks in different piezoelectric materials was crucial for the design during practical engineering intelligence. In addition, the impact load poses greater harm to the device due to the concealment of impact damage. Therefore, it is particularly important to study the mechanical behavior of interface cracks and defects in piezoelectric composite materials under impact loads [1–4].

Wang et al. [5] systematically studied the problem of Yoffe-type moving conductive cracks at the interface of two piezoelectric materials by using the complex function method. They provided an explicit expression for the field components at the interface and discussed the influence of moving cracks on the singularity of the field near the crack tip in low, medium, and high-speed states through numerical calculations. Li and Tang [6] examined the antiplane crack problem of piezoelectric composite materials. They all use integral transformation techniques to simplify mixed boundary value problems into dual singular integral equations. However, Chen and Worswick [4] discussed the effect of antiplane dynamic loading on crack propagation. In the end, they concluded that both the dynamic electric field and crack size will have an impact on the electromechanical response of dynamic loads. Wang and Yu [7] and Gu et al. [8] used the linear piezoelectric theory to study the dynamic response of a central crack perpendicular to the edge of a piezoelectric strip under antiplane mechanical and electrical impacts. They simplified the problem into a Cauchy integral equation using integral transformation and dislocation density function, and then analyzed the transient response of

load combinations, crack size on dynamic strength factor, and energy release rate through numerical examples. Zhong et al. [9] and Liu and Zhong [10] discussed the dynamic response of two collinear cracks under in-plane impact loads. They simplified the mixed initial boundary value problem using Laplace transform and Fourier transform, and finally analyzed the influence of permeable and impermeable cracks on the normalized strength factor under impact load through numerical examples. Aboudi [11] analyzed the transient electroelastic field problem caused by local defects in piezoelectric composite materials with periodic microstructures. He solved the problem using representative element method and wave propagation and compared it with the analytical solution of the transient response of piezoelectric materials with semi-infinite Type III cracks, verifying the effectiveness of this solution method. Finally, the impact of electromechanical coupling on dynamic response was analyzed through several applications. Shin and Kim [12] analyzed the transient response problem of type III interface cracks in orthotropic functional gradient/piezoelectric composite structures. They used Fourier and Laplace integral transformations to represent the problem as a second type of Fredholm integral equation, and through numerical calculations, the relevant factors were ultimately discovered, which are beneficial for preventing transient fracture of interface cracks between the piezoelectric layer and the FGOM layer. Fartash et al. [13] transformed the transient response problem of a composite piezoelectric layer containing multiple interface cracks under electromechanical impact loads into a singular integral equation problem using Fourier and Laplace transforms. They obtained expressions for the dynamic field intensity factor and dynamic energy release rate of permeable and impermeable cracks. Through numerical calculations, it was found that the interface crack geometry, electromechanical coupling, and electrical boundary conditions on the crack surface all affect the field intensity factor and dynamic energy release rate at the crack tip. Wang et al. [14] conducted experimental research on the fracture behavior of piezoelectric ceramics under impact load using high-speed photography technology. They provided the maximum voltage at the time of material fracture and combined it with finite element simulation to analyze the distribution characteristics of stress and electric field near the crack during the fracture process. Shin et al. [15] derived the transient response of cracks in the interface layer of functionally graded piezoelectric materials between two different homogeneous piezoelectric layers under antiplane shear. They found that the dynamic energy release rate increases with the increase of the material performance gradient of the functionally graded piezoelectric materials (FGPM) layer, while the electric shock load hinders crack propagation under certain conditions. At the same time, increasing the thickness of the FGPM layer can improve its transient fracture resistance. Bagheri [16] investigated the transient response problem of a piezoelectric half-plane with multiple horizontal cracks under antiplane mechanical and in-plane electrical shock. They obtained a singular integral equation system with Cauchy-type singularity using dislocation density functions and integral transformation techniques, and finally discussed the effects of geometric parameters and crack morphology on the dynamic field intensity factor. Ershad et al. [17] solved the transient response of piezoelectric coatings with several interface cracks and orthotropic functionally gradient material bands. In this study, they obtained an analytical solution for orthogonal anisotropic bands and used Fourier and Laplace integral transformations to simplify the problem into a Cauchy singularity integral equation system. Finally, they discussed the effects of geometric parameters, material properties, viscous damping, and crack arrangement on the dynamic fracture behavior of cracks. Milan and Ayatollahi [18] derived the transient response of a composite functionally graded magneto electroelastic layer with multiple interface cracks under magneto-electromechanical impact. They obtained analytical solutions for dynamic magneto-electroelastic displacement through Fourier transform and Laplace transform, and finally analyzed the effects of crack spacing and functionally gradient materials (FGM) index on dynamic intensity factor and energy release rate through numerical solution. Yang et al. [19] explored the transient response of piezoelectric material strips with parallel cracks under thermal shock and transient electrical loads. They simplified the problem into a Cauchy-type singular integral equation system by applying Laplace transform, Fourier transform, and dislocation density function. Finally, through numerical examples, it was found that the electrical load is not sensitive to the stress intensity factor but has a significant impact on the potential shift intensity factor.

From the above overview, at present, most of the theoretical research on defects in piezoelectric materials remains at the normal grain size, but there is relatively little theoretical research on interface defects in fine-grained dielectric materials [20–22]. At the same time, the mechanical, dielectric, and piezoelectric properties of fine-grained piezoelectric materials are uncertain due to differences in grain size and preparation conditions, and the relationship between them has been mostly analyzed from an experimental perspective [23, 24]. In this article, the transient behavior of multiple interface cracks in fine-grained piezoelectric coatings/substrate structures under impact loads is investigated. The interface fracture problem is transformed into a singular integral equation system problem with Cauchy kernel using Fourier and Laplace integral transformations. The field strength factor and stress distribution near the crack tip are derived, and an analytical expression for the dynamic energy release rate is constructed. Finally, the influence of various material parameters on the dynamic energy release rate is discussed through numerical calculations using the Chebyshev point placement method, which are important for the theory study of the dynamic fracture characteristics of piezoelectric intelligent composite structures.

2. Problem Formulation

Consider that the fine-grain ceramic powder was sprayed uniformly to the surface of the piezoelectric substrate by plasma spraying technology to form fine-grain piezoelectric coatings/substrate structure, as shown in Figure 1. The fine-grain piezoelectric coating and piezoelectric substrate are transversely isotropic behavior and are poled along the Z-axis. The antiplane shear impact and the electric

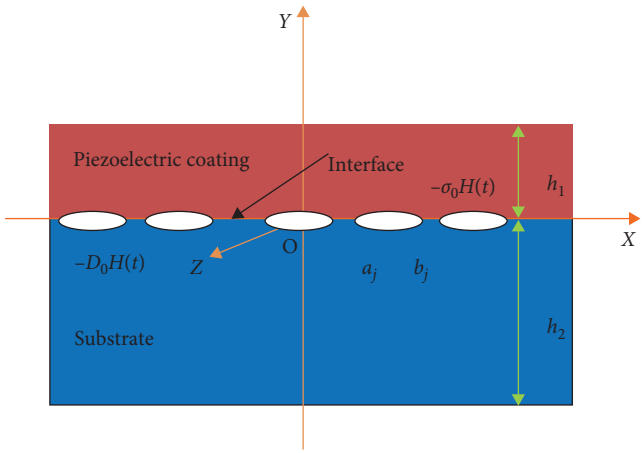

FIGURE 1: Mechanical model of multiple Griffith interface cracks between the fine-grain piezoelectric coating/substrate under impact loading.

displacement impact are imposed on the cracks surfaces. In Figure 1, the thickness of the coating is h_1 and the substrate is h_2, the multiple Griffith interface cracks all within the same orientation and occupying the intervals, $x \in (a_j, b_j)$, $(j = 1, 2, \ldots, n)$, respectively.

We consider only the out-of-plane displacement W and the in-plane electric fields Φ such that:

$$U = V = 0, W = W(x, y, t), \Phi = \Phi(x, y, t). \tag{1}$$

According to Chen and Worswick [4], the constitutive equations have the following form:

$$\sigma_{xz}(x, y, t) = c_{44}^{(k)} \frac{\partial W}{\partial x} + e_{15}^{(k)} \frac{\partial \Phi}{\partial x}, \tag{2}$$

$$D_x(x, y, t) = e_{15}^{(k)} \frac{\partial W}{\partial x} - \varepsilon_{11}^{(k)} \frac{\partial \Phi}{\partial x}, \tag{3}$$

$$\sigma_{yz}(x, y, t) = c_{44}^{(k)} \frac{\partial W}{\partial y} + e_{15}^{(k)} \frac{\partial \Phi}{\partial y}, \tag{4}$$

$$D_y(x, y, t) = e_{15}^{(k)} \frac{\partial W}{\partial y} - \varepsilon_{11}^{(k)} \frac{\partial \Phi}{\partial y}. \tag{5}$$

In Equations (2)–(5), the $\sigma_{xz}(x, y, t), \sigma_{yz}(x, y, t)$ are stress components, $D_x(x, y, t), D_y(x, y, t)$ are electric displacement components. $c_{44}^{(k)}, e_{15}^{(k)}, e_{15}^{(k)}$, and $\varepsilon_{11}^{(k)}$ are the elastic modulus, the piezoelectric, and dielectric constants, the superscript k $(k = 1, 2)$ stands for the upper and lower parts of the composite structure, respectively.

The governing equations can be written as follows:

$$c_{44}^{(k)} \nabla^2 W + e_{15}^{(k)} \nabla^2 \Phi = \rho^{(k)} \frac{\partial^2 W}{\partial t^2}, \tag{6}$$

$$e_{15}^{(k)} \nabla^2 W - \varepsilon_{11}^{(k)} \nabla^2 \Phi = 0, \ (k = 1, 2), \tag{7}$$

where ∇^2 is the double-dimensional laplacian operator, and $\rho^{(k)}$ is the mass density of the piezoelectric material.

Assume that the antiplane impact load $\sigma_0 H(t)$ and in-plane electric $D_0 H(t)$ are loaded on the surface of the Griffith interface cracks. In addition, the mixed boundary conditions of the problems can be described as follows:

$$\sigma_{yz}(x, h_1, t) = \sigma_{yz}(x, -h_2, t) = 0, \tag{8}$$

$$D_y(x, h_1, t) = D_y(x, -h_2, t) = 0, \tag{9}$$

$$\sigma_{yz}(x, 0^+, t) = \sigma_{yz}(x, 0^-, t), \ \ x \notin (a_j, b_j), \tag{10}$$

$$D_y(x, 0^+, t) = D_y(x, 0^-, t), \ \ x \notin (a_j, b_j), \tag{11}$$

$$W(x, 0^+, t) = W(x, 0^-, t), \ \ x \notin (a_j, b_j), \tag{12}$$

$$\Phi(x, 0^+, t) = \Phi(x, 0^-, t), \ \ x \notin (a_j, b_j), \tag{13}$$

$$\sigma_{yz}(x, 0^+, t) = \sigma_{yz}(x, 0^-, t) = -\sigma_0 H(t), \ \ x \in (a_j, b_j), \tag{14}$$

$$D_y(x, 0^+, t) = D_y(x, 0^-, t) = -D_0 H(t), \ \ x \in (a_j, b_j), \tag{15}$$

where σ_0, D_0 are the amplitudes and $H(t)$ is the Heaviside function.

3. Solution to the Problem

The Laplace and Fourier integral transforms of Equations (6) and (7) are given as follows:

$$W^*(x, y, \omega) = \frac{1}{2\pi} \int_{-\infty}^{+\infty} \left[A_{1k}(s, \omega) e^{|\alpha_k| y} + B_{1k}(s, \omega) e^{-|\alpha_k| y}\right] \cos(sx) ds, \tag{16}$$

$$\begin{aligned} \Phi^*(x, y, \omega) = {} & \frac{1}{2\pi} \int_{-\infty}^{+\infty} \left[A_{1k}(s, \omega) e^{|\alpha_k| y} + B_{1k}(s, \omega) e^{-|\alpha_k| y}\right] \cos(sx) ds \\ & + \frac{1}{2\pi} \int_{-\infty}^{+\infty} \left[A_{2k}(s, \omega) e^{sy} + B_{2k}(s, \omega) e^{-sy}\right] \cos(sx) ds, \end{aligned} \tag{17}$$

where

$$|\alpha_k| = \sqrt{s^2 + \left(\omega p^{(k)}\right)^2}, p^{(k)} = \sqrt{\frac{\rho^{(k)} e_{11}^{(k)}}{e_{15}^{(k)^2} + c_{44}^{(k)} e_{11}^{(k)}}}. \tag{18}$$

The quantities $A_{1k}(s, \omega), B_{1k}(s, \omega), A_{2k}(s, \omega)$, and $B_{2k}(s, \omega)$ are the unknown functions $(k = 1, 2)$ and the superscript * denotes Laplace transform.

From the constitutive Equations (4) and (5), the stress and the electric displacement are given as follows:

$$\sigma_{yz}^{*}(x,y,\omega)=\frac{1}{2\pi}\int_{-\infty}^{+\infty}\Big[\Big(c_{44}^{(k)}+e_{15}^{(k)}\Big)\big(A_{1k}(s,\omega)|\alpha_k|e^{|\alpha_k|y}-B_{1k}(s,\omega)|\alpha_k|e^{-|\alpha_k|y}\big)+e_{15}^{(k)}\big(A_{2k}(s,\omega)se^{sy}-B_{2k}(s,\omega)se^{-sy}\big)\Big]\cos(sx)ds, \tag{19}$$

$$D_{y}^{*}(x,y,\omega)=\frac{1}{2\pi}\int_{-\infty}^{+\infty}\Big[\Big(e_{15}^{(k)}+\varepsilon_{11}^{(k)}\Big)\big(A_{1k}(s,\omega)|\alpha_k|e^{|\alpha_k|y}-B_{1k}(s,\omega)|\alpha_k|e^{-|\alpha_k|y}\big)+\varepsilon_{11}^{(k)}\big(A_{2k}(s,\omega)se^{sy}-B_{2k}(s,\omega)se^{-sy}\big)\Big]\cos(sx)ds. \tag{20}$$

The mixed boundary Conditions (8)–(15) of the problems in the Laplace transform domain can be expressed as follows:

$$\sigma_{yz}^{*}(x,h_1,\omega)=\sigma_{yz}^{*}(x,-h_2,\omega)=0, \tag{21}$$

$$D_{y}^{*}(x,h_1,\omega)=D_{y}^{*}(x,-h_2,\omega)=0, \tag{22}$$

$$\sigma_{yz}^{*}(x,0^{+},\omega)=\sigma_{yz}^{*}(x,0^{-},\omega),\quad x\notin\big(a_j,b_j\big), \tag{23}$$

$$D_{y}^{*}(x,0^{+},\omega)=D_{y}^{*}(x,0^{-},\omega),\quad x\notin\big(a_j,b_j\big), \tag{24}$$

$$W^{*}(x,0^{+},\omega)=W^{*}(x,0^{-},\omega),\quad x\notin\big(a_j,b_j\big), \tag{25}$$

$$\Phi^{*}(x,0^{+},\omega)=\Phi^{*}(x,0^{-},\omega),\quad x\notin\big(a_j,b_j\big), \tag{26}$$

$$\sigma_{yz}^{*}(x,0^{+},\omega)=\sigma_{yz}^{*}(x,0^{-},\omega)=\frac{-\sigma_0}{\omega},\quad x\in\big(a_j,b_j\big), \tag{27}$$

$$D_{y}^{*}(x,0^{+},\omega)=D_{y}^{*}(x,0^{-},\omega)=\frac{-D_0}{\omega},\quad x\in\big(a_j,b_j\big). \tag{28}$$

The problem reduces to the determination of the two unknown functions. For that we introduce the density function as follows:

$$g_{W}^{*(j)}(x,\omega)=\frac{\partial}{\partial x}\big[W^{*(j)}(x,0^{+},\omega)-W^{*(j)}(x,0^{-},\omega)\big], \tag{29}$$

$$g_{\Phi}^{*(j)}(x,\omega)=\frac{\partial}{\partial x}\big[\Phi^{*(j)}(x,0^{+},\omega)-\Phi^{*(j)}(x,0^{-},\omega)\big],\ (j=1,2,\ldots,n). \tag{30}$$

From Equations (25) and (26), the dislocation density function should satisfy the following single-valued conditions:

$$\int_{a_j}^{b_j}g_{W}^{*(j)}(t,\omega)dt=0,\ g_{W}^{*(j)}(x,\omega)=0\ \text{for}\ x\notin\big(a_j,b_j\big)\ (j=1,2,\ldots,n), \tag{31}$$

$$\int_{a_j}^{b_j}g_{\Phi}^{*(j)}(t,\omega)dt=0,\ g_{\Phi}^{*(j)}(x,\omega)=0\ \text{for}\ x\notin\big(a_j,b_j\big)\ (j=1,2,\ldots,n). \tag{32}$$

From the boundary Conditions (21) and (22), we obtained the following equations:

$$A_{11}(s,\omega)=B_{11}(s,\omega)e^{-2|\alpha_1|h_1},A_{21}(s,\omega)=B_{21}(s,\omega)e^{-2|\alpha_1|h_1}, \tag{33}$$

$$B_{12}(s,\omega)=A_{12}(s,\omega)e^{-2|\alpha_2|h_2},B_{22}(s,\omega)=A_{22}(s,\omega)e^{-2|\alpha_2|h_2}. \tag{34}$$

Putting Equations (16) and (17) into Equations (29) and (30), and inserting Equations (19) and (20) into the boundary Conditions (21)–(24), (27), and (28), we get the following equations:

$$\Big(c_{44}^{(1)}+e_{15}^{(1)}\Big)\big(A_{11}(s,\omega)e^{|\alpha_1|h_1}-B_{11}(s,\omega)e^{-|\alpha_1|h_1}\big)+e_{15}^{(1)}\big(A_{21}(s,\omega)e^{|\alpha_1|h_1}-B_{21}(s,\omega)e^{-|\alpha_1|h_1}\big)=0, \tag{35}$$

$$\Big(c_{44}^{(2)}+e_{15}^{(2)}\Big)\big(A_{12}(s,\omega)e^{-|\alpha_1|h_2}-B_{12}(s,\omega)e^{|\alpha_1|h_2}\big)+e_{15}^{(2)}\big(A_{22}(s,\omega)e^{-|\alpha_1|h_2}-B_{22}(s,\omega)e^{|\alpha_1|h_2}\big)=0, \tag{36}$$

$$\Big(e_{15}^{(1)}+\varepsilon_{11}^{(1)}\Big)\big(A_{11}(s,\omega)e^{|\alpha_1|h_1}-B_{11}(s,\omega)e^{-|\alpha_1|h_1}\big)+\varepsilon_{11}^{(1)}\big(A_{21}(s,\omega)e^{|\alpha_1|h_1}-B_{21}(s,\omega)e^{-|\alpha_1|h_1}\big)=0, \tag{37}$$

$$\Big(e_{15}^{(2)}+\varepsilon_{11}^{(2)}\Big)\big(A_{12}(s,\omega)e^{-|\alpha_2|h_2}-B_{12}(s,\omega)e^{|\alpha_2|h_2}\big)-\varepsilon_{11}^{(2)}\big(A_{22}(s,\omega)e^{-|\alpha_2|h_2}-B_{22}(s,\omega)e^{|\alpha_2|h_2}\big)=0, \tag{38}$$

$$\Big(c_{44}^{(1)}+e_{15}^{(1)}\Big)(A_{11}(s,\omega)-B_{11}(s,\omega))+e_{15}^{(1)}(A_{21}(s,\omega)-B_{21}(s,\omega))=\Big(c_{44}^{(2)}+e_{15}^{(2)}\Big)(A_{12}(s,\omega)-B_{12}(s,\omega))+e_{15}^{(2)}(A_{22}(s,\omega)-B_{22}(s,\omega)), \tag{39}$$

$$\begin{aligned}&\left(e_{15}^{(1)}+\varepsilon_{11}^{(1)}\right)(A_{11}(s,\omega)-B_{11}(s,\omega))-\varepsilon_{11}^{(1)}(A_{21}(s,\omega)-B_{21}(s,\omega))\\&=\left(e_{15}^{(2)}+\varepsilon_{11}^{(2)}\right)(A_{12}(s,\omega)-B_{12}(s,\omega))-\varepsilon_{11}^{(2)}(A_{22}(s,\omega)-B_{22}(s,\omega)),\end{aligned}\tag{40}$$

$$\begin{aligned}&A_{11}(s,\omega)+B_{11}(s,\omega)-A_{12}(s,\omega)-B_{12}(s,\omega)\\&=\frac{i}{\omega}\int_{a_j}^{b_j}g_W^{*(j)}(t,\omega)e^{i\omega t}dt=G_1,\end{aligned}\tag{41}$$

$$\begin{aligned}&A_{21}(s,\omega)+B_{21}(s,\omega)-A_{22}(s,\omega)-B_{22}(s,\omega)\\&=\frac{i}{\omega}\int_{a_j}^{b_j}g_\Phi^{*(j)}(t,\omega)e^{i\omega t}dt=G_2.\end{aligned}\tag{42}$$

From linear Equations (35)–(42), we have the following equations:

$$A_{11}(s,\omega)=\frac{F_1G_1+F_2G_2}{F},\quad A_{12}(s,\omega)=\frac{F_3G_1+F_4G_2}{F},\tag{43}$$

$$B_{11}(s,\omega)=\frac{F_5G_1+F_6G_2}{F},\quad B_{12}(s,\omega)=\frac{F_7G_1+F_8G_2}{F},\tag{44}$$

$$A_{21}(s,\omega)=\frac{F_9G_1+F_{10}G_2}{F},\quad A_{22}(s,\omega)=\frac{F_{11}G_1+F_{12}G_2}{F},\tag{45}$$

$$B_{21}(s,\omega)=\frac{F_{13}G_1+F_{14}G_2}{F},\quad B_{22}(s,\omega)=\frac{F_{15}G_1+F_{16}G_2}{F}.\tag{46}$$

The expressions of F and F_q $(q=1,2,\ldots,16)$ are given in Appendix A. Where the unknown functions $A_{m1}(s,\omega)$, $A_{m2}(s,\omega)$ and $B_{m1}(s,\omega), B_{m2}(s,\omega)$ $(m=1,2)$ are depending on G_1 and G_2.

The Equations (19) and (20) can be expressed as follows:

$$\begin{aligned}\sigma_{yz}^*(x,y,\omega)=\frac{1}{2\pi}\int_{-\infty}^{+\infty}\frac{e^y}{F}\Bigg\{&\left[\left(c_{44}^{(2)}+e_{15}^{(2)}\right)|\alpha_2|e^{|\alpha_2|y}\left(F_3-F_1e^{-2|\alpha_2|y}\right)+e_{15}^{(2)}se^{sy}\left(F_{11}-F_{15}e^{-2sy}\right)\right]G_1\\&+\left[\left(c_{44}^{(2)}+e_{15}^{(2)}\right)|\alpha_2|e^{|\alpha_2|y}\left(F_4-F_8e^{-2|\alpha_2|y}\right)+e_{15}^{(2)}se^{sy}\left(F_{12}-F_{16}e^{-2sy}\right)\right]G_2\Bigg\}\cos(sx)ds,\end{aligned}\tag{47}$$

$$\begin{aligned}D_{yz}^*(x,y,\omega)=\frac{1}{2\pi}\int_{-\infty}^{+\infty}\frac{e^y}{F}\Bigg\{&\left[\left(e_{15}^{(2)}+\varepsilon_{11}^{(2)}\right)|\alpha_2|e^{|\alpha_2|y}\left(F_3-F_1e^{-2|\alpha_2|y}\right)+\varepsilon_{11}^{(2)}se^{sy}\left(F_{11}-F_{15}e^{-2sy}\right)\right]G_1\\&+\left[\left(e_{15}^{(2)}+\varepsilon_{11}^{(2)}\right)|\alpha_2|e^{|\alpha_2|y}\left(F_4-F_8e^{-2|\alpha_2|y}\right)+\varepsilon_{11}^{(2)}se^{sy}\left(F_{12}-F_{16}e^{-2sy}\right)\right]G_2\Bigg\}\cos(sx)ds.\end{aligned}\tag{48}$$

We let $y\longrightarrow 0^-$, the integral Equations (47) and (48) will be as follows:

$$\begin{aligned}\sigma_{yz}^*(x,0^-,\omega)=\frac{1}{2\pi}\lim_{y\to0^-}\int_{-\infty}^{+\infty}\frac{e^y}{F}\Bigg\{&\left[\left(c_{44}^{(2)}+e_{15}^{(2)}\right)|\alpha_2|(F_3-F_1)+e_{15}^{(2)}s(F_{11}-F_{15})\right]G_1\\&+\left[\left(c_{44}^{(2)}+e_{15}^{(2)}\right)|\alpha_2|(F_4-F_8)+e_{15}^{(2)}s(F_{12}-F_{16})\right]G_2\Bigg\}\cos(sx)ds=\frac{-\sigma_0}{\omega},\end{aligned}\tag{49}$$

$$\begin{aligned}D_{yz}^*(x,0^-,\omega)=\frac{1}{2\pi}\lim_{y\to0^-}\int_{-\infty}^{+\infty}\frac{e^y}{F}\Bigg\{&\left[\left(e_{15}^{(2)}+\varepsilon_{11}^{(2)}\right)|\alpha_2|(F_3-F_1)+\varepsilon_{11}^{(2)}s(F_{11}-F_{15})\right]G_1\\&+\left[\left(e_{15}^{(2)}+\varepsilon_{11}^{(2)}\right)|\alpha_2|(F_4-F_8)+\varepsilon_{11}^{(2)}s(F_{12}-F_{16})\right]G_2\Bigg\}\cos(sx)ds=\frac{D_0}{\omega}.\end{aligned}\tag{50}$$

Equations (49) and (50) can be described as follows:

$$\frac{1}{2\pi}\int_{-\infty}^{+\infty}\frac{e^{y}}{F}Q_1G_1\cos(sx)ds+\int_{-\infty}^{+\infty}Q_2G_2\cos(sx)ds=\frac{-\sigma_0}{\omega}, \tag{51}$$

$$\frac{1}{2\pi}\int_{-\infty}^{+\infty}\frac{e^{y}}{F}Q_3G_1\cos(sx)ds+\frac{1}{2\pi}\int_{-\infty}^{+\infty}\frac{e^{y}}{F}Q_4G_1\cos(sx)ds=\frac{D_0}{\omega}, \tag{52}$$

where

$$Q_1(s,\omega)=\left(c_{44}^{(2)}+e_{15}^{(2)}\right)|\alpha_2|(F_3-F_7)+e_{15}^{(2)}s(F_{11}-F_{15}), \tag{53}$$

$$Q_2(s,\omega)=\left(c_{44}^{(2)}+e_{15}^{(2)}\right)|\alpha_2|(F_4-F_8)+e_{15}^{(2)}s(F_{12}-F_{16}), \tag{54}$$

$$Q_3(s,\omega)=\left(e_{15}^{(2)}+\varepsilon_{11}^{(2)}\right)|\alpha_2|(F_3-F_7)+\varepsilon_{11}^{(2)}s(F_{11}-F_{15}), \tag{55}$$

$$Q_4(s,\omega)=\left(e_{15}^{(2)}+\varepsilon_{11}^{(2)}\right)|\alpha_2|(F_4-F_8)+\varepsilon_{11}^{(2)}s(F_{12}-F_{16}). \tag{56}$$

By replacing the expression of F_1 and F_2 into Equations (40) and (41), we obtained the following equations:

$$\frac{1}{2\pi}\int_{-\infty}^{+\infty}\frac{i|\alpha|Q_1e^{|\alpha|y}}{\alpha H}\left(\int_{a_j}^{b_j}g_W^{*(j)}(t)e^{i\alpha t}dt\right)e^{-i\alpha x}d\alpha+\frac{1}{2\pi}\int_{-\infty}^{+\infty}\frac{|\alpha|Q_2e^{|\alpha|y}}{\alpha H}\left(\int_{a_j}^{b_j}g_\Phi^{*(j)}(t)e^{i\alpha t}dt\right)e^{-i\alpha x}d\alpha=-\sigma_0, \tag{57}$$

$$\frac{1}{2\pi}\int_{-\infty}^{+\infty}\frac{i|\alpha|Q_3e^{|\alpha|y}}{\alpha H}\left(\int_{a_j}^{b_j}g_W^{*(j)}(t)e^{i\alpha t}dt\right)e^{-i\alpha x}d\alpha+\frac{1}{2\pi}\int_{-\infty}^{+\infty}\frac{|\alpha|Q_4e^{|\alpha|y}}{\alpha H}\left(\int_{a_j}^{b_j}g_\Phi^{*(j)}(t)e^{i\alpha t}dt\right)e^{-i\alpha x}d\alpha=-D_0. \tag{58}$$

Through Equations (51)–(58), on the surface of the crack, we obtain the following coupled the first kind Cauchy singular integral equations:

$$\int_{a_j}^{b_j}\left(\frac{Q_{1*}}{F_*}\frac{1}{t-x}+k_1(x,t,\omega)\right)g_W^{*(j)}(t,\omega)dt+\int_{a_j}^{b_j}\left(\frac{Q_{2*}}{F_*}\frac{1}{t-x}+k_2(x,t,\omega)\right)g_\Phi^{*(j)}(t,\omega)dt=-\frac{\pi\sigma_0}{\omega}, \tag{59}$$

$$\int_{a_j}^{b_j}\left(\frac{Q_{3*}}{F_*}\frac{1}{t-x}+k_3(x,t,\omega)\right)g_W^{*(j)}(t,\omega)dt+\int_{a_j}^{b_j}\left(\frac{Q_{4*}}{F_*}\frac{1}{t-x}+k_4(x,t,\omega)\right)g_\Phi^{*(j)}(t,\omega)dt=-\frac{\pi D_0}{\omega}. \tag{60}$$

The expressions of F_*, Q_{m*}, and $k_m(x,t,\omega)$, $(m=1,2,3,4)$ are given in Appendix B. In these equations, $g_W^{*(j)}(t,\omega)$ and $g_\Phi^{*(j)}(t,\omega)$ are unknown functions with the following single-valued condition:

$$\int_{a_j}^{b_j}g_W^{*(j)}(t,\omega)dt=0 \text{ and } \int_{a_j}^{b_j}g_\Phi^{*(j)}(t,\omega)dt=0,\quad (j=1,2,\ldots,n). \tag{61}$$

By the principle of superposition and mixed boundary conditions, Equations (59) and (60) can be formulated as follows:

$$\sum_{j=1}^{n}\left(\int_{a_j}^{b_j}\left(\frac{Q_{1*}}{F_*}\frac{1}{t_j-x_k}+k_1(x_k,t_j,\omega)\right)g_W^{*(j)}(t_j,\omega)dt_j+\int_{a_j}^{b_j}\left(\frac{Q_{2*}}{F_*}\frac{1}{t_j-x_k}+k_2(x_k,t_j,\omega)\right)g_\Phi^{*(j)}(t_j,\omega)dt_j\right)=-\frac{\pi\sigma_0}{\omega}, \tag{62}$$

$$\sum_{j=1}^{n}\int_{a_j}^{b_j}\left(\frac{Q_{3*}}{F_*}\frac{1}{t_j-x_k}+k_3(x_k,t_j,\omega)\right)g_W^{*(j)}(t_j,\omega)dt_j+\int_{a_j}^{b_j}\left(\frac{Q_{4*}}{F_*}\frac{1}{t_j-x_k}+k_4(x_k,t_j,\omega)\right)g_\Phi^{*(j)}(t_j,\omega)dt_j=-\frac{\pi D_0}{\omega}\quad (x_k\in(a_k,b_k),j,k=1,2,\ldots,n). \tag{63}$$

4. Resolution of Singular Integral Equations

4.1. Normalization of Singular Integral Equations. According to Gu et al. [8], the singular integral Equations (62) and (63) are transformed into as follows:

$$\sum_{j=1}^{n}\left(\int_{-1}^{1}\left(\frac{Q_{1*}}{F_*}\frac{a_{0j}}{a_{0j}s_j+c_{0j}-a_{0k}r_k-c_{0k}}+a_{0j}L_1\left(r_k,s_j,\omega\right)\right)f_1^{(j)}\left(s_j,\omega\right)ds_j\right.$$
$$\left.+\int_{-1}^{1}\left(\frac{Q_{2*}}{F_*}\frac{a_{0j}}{a_{0j}s_j+c_{0j}-a_{0k}r_k-c_{0k}}+a_{0j}L_2\left(r_k,s_j,\omega\right)\right)f_2^{(j)}\left(s_j,\omega\right)ds_j\right)=-\pi\sigma_0, \tag{64}$$

$$\sum_{j=1}^{n}\left(\int_{-1}^{1}\left(\frac{Q_{3*}}{F_*}\frac{a_{0j}}{a_{0j}s_j+c_{0j}-a_{0k}r_k-c_{0k}}+a_{0j}L_3\left(r_k,s_j,\omega\right)\right)f_1^{(j)}\left(s_j\right)ds_j\right.$$
$$\left.+\int_{-1}^{1}\left(\frac{Q_{4*}}{F_*}\frac{a_{0j}}{a_{0j}s_j+c_{0j}-a_{0k}r_k-c_{0k}}+a_{0j}L_4\left(r_k,s_j,\omega\right)\right)f_2^{(j)}\left(s_j\right)ds_j\right)=-\pi D_0. \tag{65}$$

Based on the numerical method, the dislocation density functions $f_1^{(j)}(s_j)$ and $f_2^{(j)}(s_j)$ $(j=1,2,\ldots,n)$ in Equations (64) and (65) are expressed as follows:

$$f_1^{(j)}\left(s_j,\omega\right)=\frac{g_1^{(j)}\left(s_j,\omega\right)}{\omega\sqrt{1-s_j^2}}\pi\sigma_0, \tag{66}$$

$$f_2^{(j)}\left(s_j,\omega\right)=\frac{g_2^{(j)}\left(s_j,\omega\right)}{\omega\sqrt{1-s_j^2}}\pi D_0,\ \ (j=1,2,\ldots,n), \tag{67}$$

where $r_j, s_j f_1^{(j)}(x,\omega), f_2^{(j)}(x,\omega), L_i(r,s,\omega), a_{0j}$, and c_{0j} $(i=1,2,3,4)$, $(j=1,2,\ldots,n)$ are given in Appendix C. $g_1^{(j)}(s_j,\omega)$ and $f_2^{(j)}(s_j,\omega)$ are continuous function defined in the interval $[-1,1]$.

According to Erdogan et al. [25], the Guss–Chebyshev collocation method can be used to solve Equations (64) and (65). Transform Equations (64)–(67) into the system of algebraic equations:

$$\frac{1}{N}\sum_{R=0}^{N}\chi_R\sum_{j=1}^{n}\left[\left(\frac{Q_{1*}}{F_*}\frac{a_{0j}}{a_{0j}s_{jR}+c_{0j}-a_{0k}r_{kq}-c_{0k}}+a_{0j}L_1\left(r_{kq},s_{jR},\omega\right)\right)g_1^{(j)}\left(s_{jR},\omega\right)\right.$$
$$\left.+\left(\frac{Q_{2*}}{F_*}\frac{a_{0j}}{a_{0j}s_{jR}+c_{0j}-a_{0k}r_{kq}-c_{0k}}+a_{0j}L_2\left(r_{kq},s_{jR},\omega\right)\right)g_2^{(j)}\left(s_{jR},\omega\right)\right]=-1, \tag{68}$$

$$\frac{1}{N}\sum_{R=0}^{N}\chi_R\sum_{j=1}^{n}\left[\left(\frac{Q_{3*}}{F_*}\frac{a_{0j}}{a_{0j}s_{jR}+c_{0j}-a_{0k}r_{kq}-c_{0k}}+a_{0j}L_3\left(r_{kq},s_{jR},\ \omega\right)\right)g_1^{(j)}\left(s_{jR},\ \omega\right)\right.$$
$$\left.+\left(\frac{Q_{4*}}{F_*}\frac{a_{0j}}{a_{0j}s_{jR}+c_{0j}-a_{0k}r_{kq}-c_{0k}}+a_{0j}L_4\left(r_{kq},s_{jR},\ \omega\right)\right)g_2^{(j)}\left(s_{jR},\ \omega\right)\right]=-1, \tag{69}$$

$$\sum_{R=0}^{N}\chi_R g_1^{(k)}(s_{kR},\omega)=0,\ \sum_{R=0}^{N}\chi_R g_2^{(k)}(s_{kR},\omega)=0, \tag{70}$$

where

$$\chi_0=\chi_N=\frac{1}{2},\chi_1=,\ldots,=\chi_{N-1}=1, \tag{71}$$

$$r_{kq}=\cos\frac{(2q-1)\pi}{2N},\ s_{jR}=\cos\frac{R\pi}{N}, \tag{72}$$

$$k=1,2,\ldots,n,q=1,2,\ldots,N, \tag{73}$$

where N is the node number of quadrature formula, s_{jR} and r_{kq} are the zero points of the first and second kinds of Chebyshev polynomials. Once solving Equations (68)–(70) numerically to get the solutions of $g_1^{(j)}(s_j,\omega)$ and $g_2^{(j)}(s_j,\omega)$, which can permit to get the stress and electric displacement.

4.2. Fracture Parameters. The intensity factors in Laplace transform domain are defined by Chen and Worswick [4]:

$$K_\sigma^{*a_j}=\lim_{x\to a_j^-}\sqrt{2\pi(a_j-x)}\,\sigma_{yz}^*(x,0,\omega), \tag{74}$$

$$K_\sigma^{*b_j}=\lim_{x\to b_j^+}\sqrt{2\pi(x-b_j)}\,\sigma_{yz}^*(x,0,\omega), \tag{75}$$

$$K_D^{*a_j}=\lim_{x\to a_j^-}\sqrt{2\pi(a_j-x)}\,D_y^*(x,0,\omega), \tag{76}$$

$$K_D^{*b_j}=\lim_{x\to b_j^+}\sqrt{2\pi(x-b_j)}\,D_y^*(x,0,\omega),\ j=1,2,\ldots,n. \tag{77}$$

From Equations (59) and (60), the singular part of $\sigma_{yz}^*(x,0,\omega)$ and $D_y^*(x,0,\omega)$ are expressed as follows:

$$\begin{aligned}\lim_{x\to a_j^-}\sigma_{yz}^*(x,0,\omega)&=\frac{Q_{1*}}{F_*}\lim_{s_j\to-1^-}\int_{-1}^{1}\frac{f_1^{(1)}(s_j,\omega)}{s_j-x_j}ds_j\\&+\frac{Q_{2*}}{F_*}\lim_{s_j\to-1^-}\int_{-1}^{1}\frac{f_2^{(1)}(s_j,\omega)}{s_j-x_j}ds_j,\end{aligned} \tag{78}$$

$$\begin{aligned}\lim_{x\to a_j^-}D_y^*(x,0,\omega)&=\frac{Q_{3*}}{F_*}\lim_{s_j\to-1^-}\int_{-1}^{1}\frac{f_1^{(1)}(s_j,\omega)}{s_j-x_j}ds_j\\&+\frac{Q_{4*}}{F_*}\lim_{s_j\to-1^-}\int_{-1}^{1}\frac{f_2^{(1)}(s_j,\omega)}{s_j-x_j}ds_j,\end{aligned} \tag{79}$$

$$\begin{aligned}\lim_{x\to b_j^+}\sigma_{yz}^*(x,0,\omega)&=\frac{Q_{1*}}{F_*}\lim_{s_j\to1^+}\int_{-1}^{1}\frac{f_1^{(1)}(s_j,\omega)}{s_j-x_j}ds_j\\&+\frac{Q_{2*}}{F_*}\lim_{s_j\to1^+}\int_{-1}^{1}\frac{f_2^{(1)}(s_j,\omega)}{s_j-x_j}ds_j,\end{aligned} \tag{80}$$

$$\begin{aligned}\lim_{x\to b_j^+}D_y^*(x,0,\omega)&=\frac{Q_{3*}}{F_*}\lim_{s_j\to1^+}\int_{-1}^{1}\frac{f_1^{(1)}(s_j,\omega)}{s_j-x_j}ds_j\\&+\frac{Q_{4*}}{F_*}\lim_{s_j\to1^+}\int_{-1}^{1}\frac{f_2^{(1)}(s_j,\omega)}{s_j-x_j}ds_j.\end{aligned} \tag{81}$$

Substituting Equations (66) and (67) into Equations (78)–(81), we obtain the following equations:

$$\begin{aligned}\lim_{x\to a_j^-}\sigma_{yz}^*(x,0,\omega)&=\frac{\sigma_0Q_{1*}}{F_*}\lim_{s_j\to-1^-}\frac{g_1^{(j)}(-1,\omega)}{\sqrt{s_j^2-1}}\\&+\frac{\sigma_0Q_{2*}}{F_*}\lim_{s_j\to-1^-}\frac{g_2^{(j)}(-1,\omega)}{\sqrt{s_j^2-1}},\end{aligned} \tag{82}$$

$$\begin{aligned}\lim_{x\to b_j^+}\sigma_{yz}^*(x,0,\omega)&=\frac{\sigma_0Q_{1*}}{F_*}\lim_{s_j\to1^+}\frac{-g_1^{(j)}(1,\omega)}{\sqrt{s_j^2-1}}\\&+\frac{\sigma_0Q_{2*}}{F_*}\lim_{s_j\to-1^-}\frac{-g_2^{(j)}(1,\omega)}{\sqrt{s_j^2-1}},\end{aligned} \tag{83}$$

$$\begin{aligned}\lim_{x\to a_j^-}D_y^*(x,0,\omega)&=\frac{D_0Q_{3*}}{F_*}\lim_{s_j\to-1^-}\frac{g_1^{(j)}(-1,\omega)}{\sqrt{s_j^2-1}}\\&+\frac{D_0Q_{4*}}{F_*}\lim_{s_j\to-1^-}\frac{g_2^{(j)}(-1,\omega)}{\sqrt{s_j^2-1}},\end{aligned} \tag{84}$$

$$\begin{aligned}\lim_{x\to b_j^+}D_y^*(x,0,\omega)&=\frac{D_0Q_{3*}}{F_*}\lim_{s_j\to1^+}\frac{-g_1^{(j)}(1,\omega)}{\sqrt{s_j^2-1}}\\&+\frac{D_0Q_{4*}}{F_*}\lim_{s_j\to-1^-}\frac{-g_2^{(j)}(1,\omega)}{\sqrt{s_j^2-1}}.\end{aligned} \tag{85}$$

Inserting Equations (82)–(85) into Equations (79)–(81), we get the following equations:

$$K_\sigma^{*a_j}=\sigma_0\sqrt{\pi a_{0j}}\left[\frac{Q_{1*}}{F_*}g_1^{(j)}(-1,\omega)+\frac{Q_{2*}}{F_*}g_2^{(j)}(-1,\omega)\right], \tag{86}$$

$$K_\sigma^{*b_j}=-\sigma_0\sqrt{\pi a_{0j}}\left[\frac{Q_{1*}}{F_*}g_1^{(j)}(1,\omega)+\frac{Q_{2*}}{F_*}g_2^{(j)}(1,\omega)\right], \tag{87}$$

$$K_D^{*a_j}=D_0\sqrt{\pi a_{0j}}\left[\frac{Q_{3*}}{F_*}g_1^{(j)}(-1,\omega)+\frac{Q_{4*}}{F_*}g_2^{(j)}(-1,\omega)\right], \tag{88}$$

$$K_D^{*b_j}=-D_0\sqrt{\pi a_{0j}}\left[\frac{Q_{3*}}{F_*}g_1^{(j)}(1,\omega)+\frac{Q_{4*}}{F_*}g_2^{(j)}(1,\omega)\right]. \tag{89}$$

From the inverse Laplace transform of Equations (86)–(89), the intensity factors in the time domain can be obtained as follows:

$$K_\sigma^{a_j}(t) = \sigma_0\sqrt{\pi a_{0j}}\left[\frac{Q_{1*}}{F_*}M_1^{(j)}(t) + \frac{Q_{2*}}{F_*}M_2^{(j)}(t)\right], \tag{90}$$

$$K_\sigma^{b_j}(t) = -\sigma_0\sqrt{\pi a_{0j}}\left[\frac{Q_{1*}}{F_*}M_3^{(j)}(t) + \frac{Q_{2*}}{F_*}M_4^{(j)}(t)\right], \tag{91}$$

$$K_D^{a_j}(t) = D_0\sqrt{\pi a_{0j}}\left[\frac{Q_{3*}}{F_*}M_1^{(j)}(t) + \frac{Q_{4*}}{F_*}M_2^{(j)}(t)\right], \tag{92}$$

$$K_D^{b_j}(t) = -D_0\sqrt{\pi a_{0j}}\left[\frac{Q_{3*}}{F_*}M_3^{(j)}(t) + \frac{Q_{4*}}{F_*}M_4^{(j)}(t)\right], \tag{93}$$

where

$$\begin{aligned} M_1^{(j)}(t) &= \frac{1}{2\pi i}\int_{\beta-i\infty}^{\beta+i\infty} g_1^{(j)}(-1,\omega)e^{\omega t}d\omega,\ M_2^{(j)}(t) \\ &= \frac{1}{2\pi i}\int_{\beta-i\infty}^{\beta+i\infty} g_2^{(j)}(-1,\omega)e^{\omega t}d\omega, \end{aligned} \tag{94}$$

$$\begin{aligned} M_3^{(j)}(t) &= \frac{1}{2\pi i}\int_{\beta-i\infty}^{\beta+i\infty} g_1^{(j)}(1,\omega)e^{\omega t}d\omega,\ M_4^{(j)}(t) \\ &= \frac{1}{2\pi i}\int_{\beta-i\infty}^{\beta+i\infty} g_2^{(j)}(1,\omega)e^{\omega t}d\omega. \end{aligned} \tag{95}$$

The functions $g_1^{(j)}(\pm 1,\omega)$ and $g_2^{(j)}(\pm 1,\omega)$ can be calculated from Equations (68)–(70).

From Gu et al. [8], the energy release rate of piezoelectric material has the following form:

$$G = \frac{1}{4}[\lambda_1 K_\sigma^2 + \lambda_2 K_\sigma K_D + \lambda_3 K_D^2], \tag{96}$$

where

$$\lambda_1 = \frac{Q_{4*}}{F_*\Delta}, \lambda_2 = \frac{Q_{3*} - Q_{1*}}{F_*\Delta}, \lambda_3 = \frac{-Q_{1*}}{F_*\Delta}, \Delta = \begin{bmatrix} \frac{Q_{1*}}{F_*} & \frac{Q_{2*}}{F_*} \\ \frac{Q_{3*}}{F_*} & \frac{Q_{4*}}{F_*} \end{bmatrix}. \tag{97}$$

5. Results and Discussion

In this section, we select PZT-5 piezoelectric ceramics as the base material and fine-grained PZT-5 piezoelectric ceramics as the coating material. PZT-5 material parameters are given as follows:

$$e_{15}^{(2)} = 12.3\ \text{C/m}^2, \varepsilon_{11}^{(2)} = 8.1103\times 10^{-9}\ \text{C/Vm}, \tag{98}$$

$$c_{44}^{(2)} = 2.11\times 10^{10}\ \text{N/m}^2, \rho^{(2)} = 7.75\times 10^3\ \text{kg/m}^2. \tag{99}$$

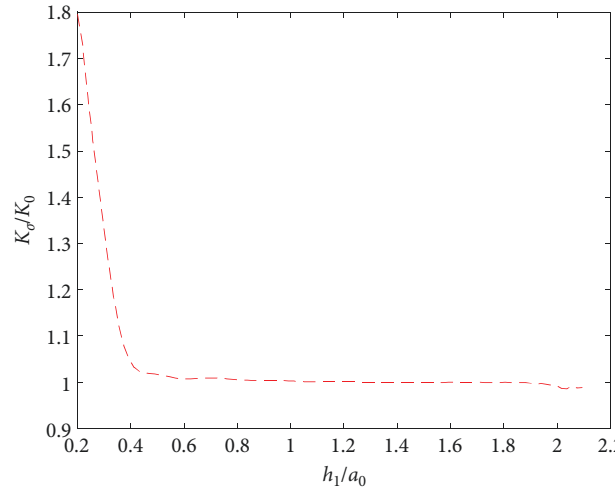

FIGURE 2: Variation of K_σ/K_0 at the crack tip with h_1/a_0.

5.1. The Single Interface Crack. In this part, to analyze the influence of material parameters on the normalized dynamic energy release rate, we selected the parameters as follows:

$c_{44}^{(1)}/c_{44}^{(2)} = 2.5$, $h_1 = 1$ mm, $h_1/h_2 = 1/100$, $a_0 = 5$ mm, the antiplane stress $\sigma_0 = 4.2$ Mpa, and the $D_0 = 10^{-3}$ c/m^2. The electromechanical coupling factor is defined as $\xi = \frac{D_0 e_{15}}{\sigma_0 \varepsilon_{11}}$.

According to Pak [1], G_0 and t_0 are given by the following expressions:

$$\begin{aligned} G_0 &= \frac{\pi l_0}{2}\frac{\varepsilon_{11}^{(2)}\sigma_0^2}{c_{44}^{(1)}\varepsilon_{11}^{(2)} + \left(e_{11}^{(1)}\right)^2}, \\ t_0 &= \sqrt{\frac{(l_0)^2\left(c_{44}^{(2)}\varepsilon_{11}^{(2)} + \left(e_{11}^{(2)}\right)^2\right)}{\rho^{(2)}\varepsilon_{11}^{(2)}}}, \end{aligned} \tag{100}$$

$$K_0 = \sigma\sqrt{a_0}. \tag{101}$$

To check the validity of analysis, the normalized stress intensity factors versus h_1/a is plotted (Figure 2).

The normalized stress intensity factors as a function of h_1/a_0 are plotted in Figure 2. Figure 2 displays the normalized stress intensity factors with h_1/a_0 for fine-grained piezoelectric coating/substrate with single interface permeable crack tips. It is observed that the normalized stress intensity factors at the left and right tips of the same crack remain consistent. Meanwhile, as h_1/a_0 increases the normalized stress intensity factors gradually decrease and eventually tend to a static value, which is consistent with the literature [6].

Next, we select $h_1 = 1$ mm, $h_1/h_2 = 1/100$, and $c_{44}^{(1)}/c_{44}^{(2)} = 2.5$ to change the size of the single interface crack, and Figure 3 is plotted.

Finally, maintaining $h_1 = 1$ mm, $h_1/h_2 = 1/100$, and $a_0 = 5$ mm, the influence of different elastic modulus ratios on the normalized dynamic energy release rate was plotted by changing the ratio of elastic modulus (Figure 4).

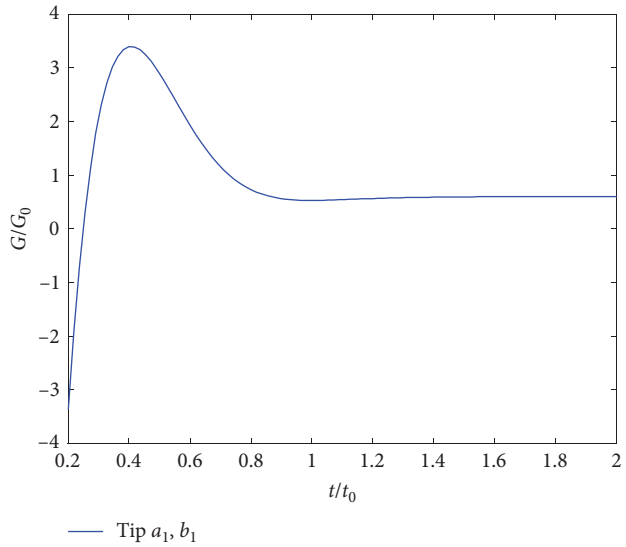

FIGURE 3: Variation of G/G_0 at the crack tip with normalization time t/t_0.

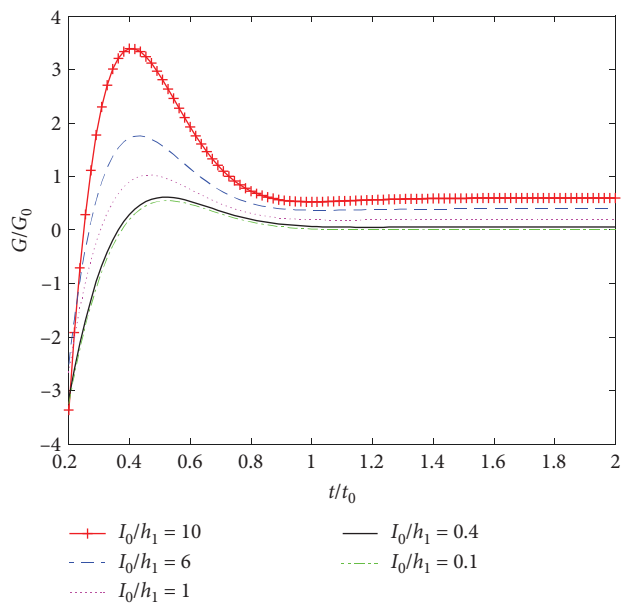

FIGURE 4: Variation of G/G_0 with t/t_0 under different cracks size.

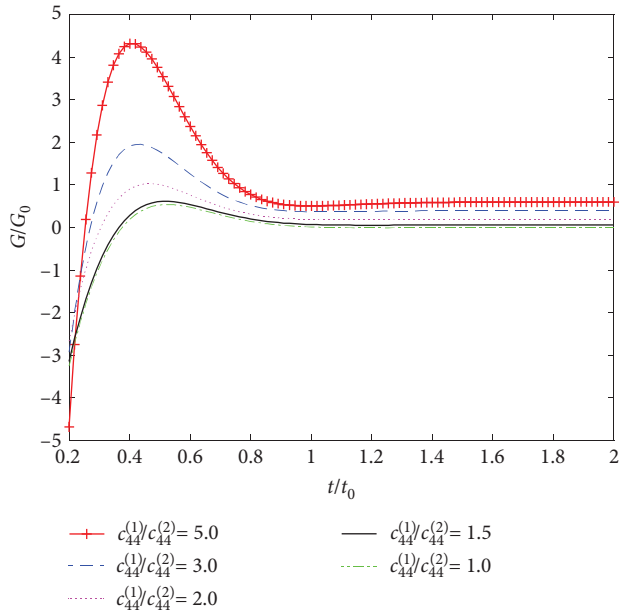

FIGURE 5: Variation of G/G_0 with t/t_0 under different elastic modulus.

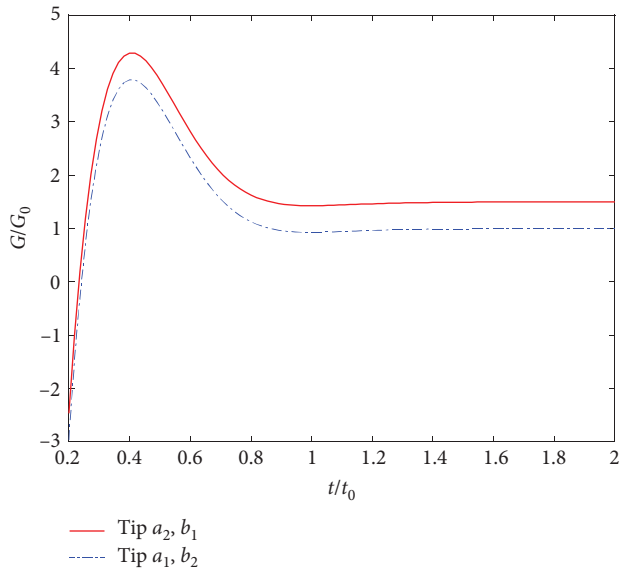

FIGURE 6: Variation of G/G_0 with t/t_0 under double consistent interface cracks.

Figure 3 shows the variation of the normalized dynamic energy release rate with t/t_0 for fine-grained piezoelectric coating/substrate with single interface permeable crack tips. It is observed that the dynamic energy release rate at the left and right tips of the same crack remains consistent. Meanwhile, as t/t_0 increases the dynamic energy release rate first increases to high values and then decreases and finally tends to static value.

Figure 4 displays the normalized dynamic energy release rate of a fine-grained piezoelectric coating/substrate versus normalized time t/t_0 for different crack sizes. It can be seen that the trends of dynamic energy release rates are similar for different crack sizes, and the time to maintain the peak value appears between $t/t_0 = 0.4 \sim 0.5$. However, as the crack size increases, the corresponding peak also increases.

Figure 5 illustrates the effect of the elastic modulus of the material on the normalized dynamic energy release rate as it changes with t/t_0. It is observed that when the coating and substrate are of the same material (i.e., $c_{44}^{(1)}/c_{44}^{(2)} = 1$), a similar conclusion was obtained in [13]. Moreover, as the ratio of material elastic modulus increases, the peak value of normalized dynamic energy release rate also increases accordingly. It is worth mentioning that when the normalization time $t/t_0 < 0.4$, the dynamic energy release rate increases rapidly.

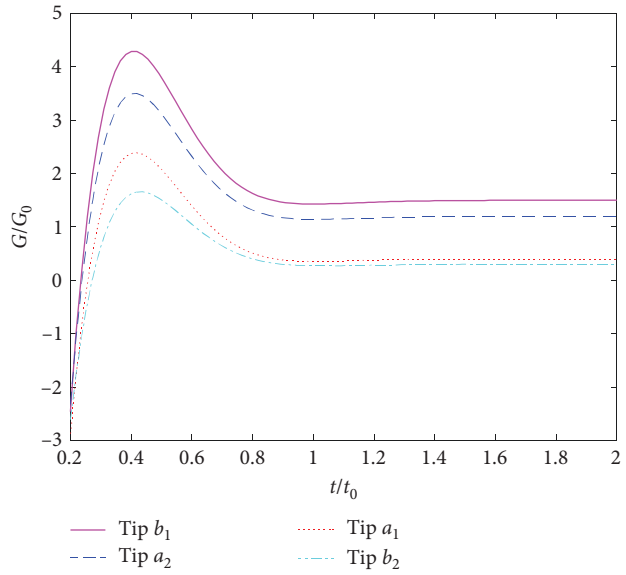

FIGURE 7: Variation of G/G_0 with t/t_0 under double inconsistent interface cracks.

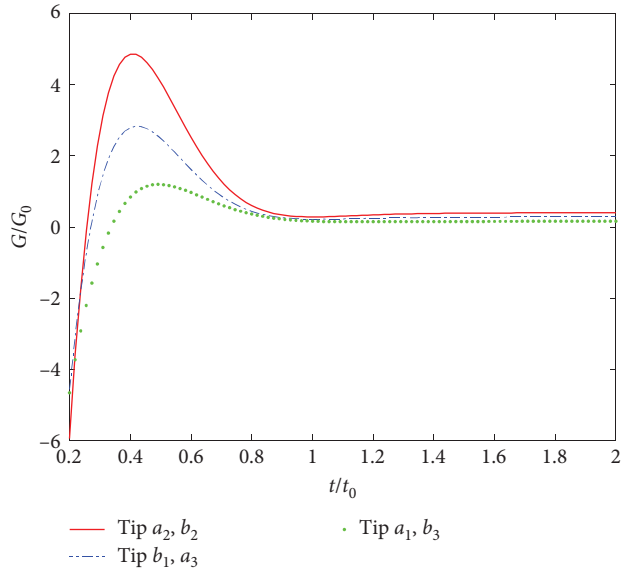

FIGURE 8: Variation of G/G_0 with t/t_0 under three identical interface cracks.

When $t/t_0 > 0.8$, the dynamic energy release rate gradually tends to astatic value.

5.2. Multiple Interface Cracks. In this section, we choose $c_{44}^{(1)}/c_{44}^{(2)} = 2.5$, $h_1 = 1$ mm, $h_1/h_2 = 1/100$, and we let the load conditions and expressions for G_0 and t_0 be consistent with the single crack case. The double interface cracks of $a_0 =$ 5 mm. In the case of inconsistent size of double interface cracks, select $a_1 = 10, a_2 = 5$ mm (Figures 6 and 7). In the three interface cracks, when the crack size is consistent, select $a_0 =$ 5 mm, and when the size is inconsistent, $a_1 = 12, a_2 = 8, a_3 =$ 5 mm (Figures 8 and 9).

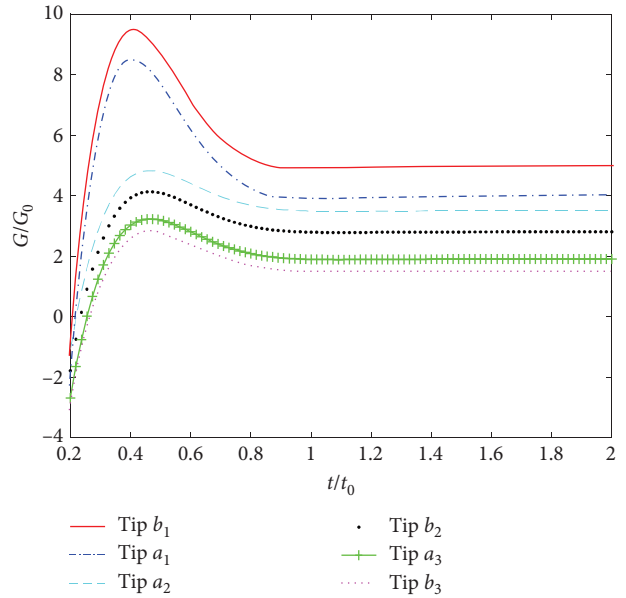

FIGURE 9: Variation of G/G_0 with t/t_0 under three inconsistent interface cracks.

Figures 6 and 7 demonstrate the variation of the normalized dynamic energy release rate with t/t_0 for fine-grained piezoelectric coating/substrate with double interface crack tips. From the figures, it can be seen that the normalized dynamic energy release rate at the tip of double interface crack is similar to that of single interface crack. As normalization time t/t_0 increases, it first increases sharply, then decreases, and finally tends to a static value. However, the peak value of the dynamic energy release rate corresponding to the tips of double interface cracks is greater than that corresponding to a single interface crack. Moreover, when the sizes of double cracks are not consistent, the crack tips near the inside of the two cracks also exhibit a higher peak energy release rate than the external crack tips. The above analysis indicates that the number and shape of cracks have a significant impact on the dynamic energy release rate.

Figures 8 and 9 display the variation of the normalized dynamic energy release rate with t/t_0 for fine-grained piezoelectric coating/substrate with three interface crack tips. It is obvious from the obtained results that the peak normalized dynamic energy release rate of the three interface crack tips is higher than that of one or two interface crack tips. As expected, the variation of normalized energy release rate with the normalization t/t_0 is consistent with the previous conclusion. At the same time, when the structure has multiple interface cracks, the peak of normalized dynamic energy release rate near the internal tip is higher than that near the external tips.

In addition, an imagination is found in Figures 3–8 that during the initial stage of impact load and electric field loading, the dynamic energy release rate shows a negative value which indicates that the electromechanical coupling factor ξ (where $\xi = 0.36$) at this time delayed the propagation of cracks. But when the normalization time $t/t_0 > 0.25$, the dynamic energy release rate gradually increases to a positive

value and shows a trend of first increasing and then decreasing with the increase of normalization time, finally tends to a steady state. The results indicate that appropriate electromechanical coupling factor can delay or promote crack propagation at different loading stages.

6. Conclusions

In this paper, the transient response of the fine-grained piezoelectric/substrate structure with multiple interface cracks under the electromechanical impact loading is investigated. The effects of material parameters, impact load, number of cracks, and crack size on the normalized dynamic energy release rate are displayed through numerical examples. The study implies that:

(1) When $t/t_0 < 0.4$, the normalized energy release rate rapidly increases to its peak. As t/t_0 continues to increase, the normalized energy release rate gradually decreases and eventually tends to a static value, and the crack size has a very significant effect on the normalized energy release rate.

(2) When changing the elastic modulus ratio of the material, the trend of normalized dynamic energy release rate with normalization time t/t_0 remains relatively unchanged, but its peak value has significant changes. The magnitude of the elastic modulus also has a significant impact on the dynamic energy release rate, and the results show that fine-grained piezoelectric materials have better structural properties than normal size materials.

(3) When the numbers of cracks are two or three, the trend of normalized dynamic energy release rate with normalization time t/t_0 is similar to that of a single crack, but a significant increase in its peak value is observed. These indicate that the numbers of cracks have a significant impact on it. At the same time, when the size of multiple cracks is inconsistent, the peak value of normalized dynamic energy release rate also exhibits different phenomena compared to the case of consistent size.

Appendix

A. Unknown Function Structure Expression

The expressions in $A_{m1}(s,\omega)$, $A_{m2}(s,\omega)$, and $B_{m1}(s,\omega)$, $B_{m2}(s,\omega)$ $(m=1,2)$ are as follows:

$$F = a_2a_3 - a_1a_4, \tag{A.1}$$

$$F_1 = \frac{e^{-2|\alpha_1|h_1}(a_2a_3 - a_1a_4) + e^{-2|\alpha_1|h_1}\left(1+e^{-2|\alpha_1|h_1}\right)\left(1-e^{-4|\alpha|h_1}\right)\left[\left(c_{44}^{(1)} + e_{15}^{(1)}\right)a_4 - e_{15}^{(1)}a_2\right]}{\left(1+e^{-2|\alpha_1|h_1}\right)}, \tag{A.2}$$

$$F_2 = \frac{e^{-2|\alpha_1|h_1}\left(1+e^{-2|\alpha_1|h_1}\right)\left(1-e^{-4|\alpha_1|h_1}\right)\left[\left(e_{15}^{(2)} + \varepsilon_{11}^{(2)}\right)a_4 - \varepsilon_{11}^{(1)}a_3\right]}{\left(1+e^{-2|\alpha_1|h_1}\right)}, \tag{A.3}$$

$$F_3 = \left(1-e^{-4|\alpha_1|h_1}\right)\left[\left(c_{44}^{(1)} + e_{15}^{(1)}\right)a_3 - e_{15}^{(1)}a_2\right], \tag{A.4}$$

$$F_4 = \left(1-e^{-4|\alpha_1|h_1}\right)\left[\left(e_{15}^{(2)} + \varepsilon_{11}^{(2)}\right)a_4 - \varepsilon_{11}^{(1)}a_3\right], \tag{A.5}$$

$$F_5 = \frac{a_2a_3 - a_1a_4 + \left(1+e^{-2|\alpha_1|h_1}\right)\left(1-e^{-4|\alpha_1|h_1}\right)\left[\left(c_{44}^{(1)} + e_{15}^{(1)}\right)a_4 - e_{15}^{(1)}a_2\right]}{\left(1+e^{-2|\alpha_1|h_1}\right)}, \tag{A.6}$$

$$F_6 = \frac{\left(1+e^{-2|\alpha_1|h_1}\right)\left(1-e^{-4|\alpha_1|h_1}\right)\left[\left(e_{15}^{(2)} + \varepsilon_{11}^{(2)}\right)a_4 - \varepsilon_{11}^{(1)}a_3\right]}{\left(1+e^{-2|\alpha_1|h_1}\right)}, \tag{A.7}$$

$$F_7 = e^{-2|\alpha_2|h_2}\left(1-e^{-4|\alpha_1|h_1}\right)\left[\left(c_{44}^{(1)} + e_{15}^{(1)}\right)a_3 - e_{15}^{(1)}a_2\right], \tag{A.8}$$

$$F_8 = e^{-2|\alpha_2|h_2}\left(1 - e^{-4|\alpha_1|h_1}\right)\left[\left(e_{15}^{(2)} + \varepsilon_{11}^{(2)}\right)a_4 - \varepsilon_{11}^{(1)}a_3\right], \tag{A.9}$$

$$F_9 = \frac{e^{-2|\alpha_1|h_1}(a_2a_3 - a_1a_4) + e^{-2|\alpha_1|h_1}\left(1 + e^{-2|\alpha_1|h_1}\right)\left(1 - e^{-4|\alpha_1|h_1}\right)\left[\left(e_{15}^{(1)} + \varepsilon_{11}^{(1)}\right)a_1 - \left(c_{44}^{(1)} + e_{15}^{(1)}\right)a_2\right]}{\left(1 + e^{-2|\alpha_1|h_1}\right)}, \tag{A.10}$$

$$F_{10} = \frac{e^{-2|\alpha_1|h_1}\left(1 + e^{-2|\alpha_1|h_1}\right)\left(1 - e^{-4|\alpha_1|h_1}\right)\left[\left(e_{15}^{(1)} + \varepsilon_{11}^{(1)}\right)a_1 - e_{15}^{(1)}a_2\right]}{\left(1 + e^{-2|\alpha_1|h_1}\right)}, \tag{A.11}$$

$$F_{11} = \left(1 - e^{-4|\alpha_1|h_1}\right)\left[\left(e_{15}^{(1)} + \varepsilon_{11}^{(1)}\right)a_1 - \left(c_{44}^{(1)} + e_{15}^{(1)}\right)a_2\right], \tag{A.12}$$

$$F_{12} = \left(1 - e^{-4|\alpha_1|h_1}\right)\left(\left(e_{15}^{(1)} + \varepsilon_{11}^{(1)}\right)a_1 - e_{15}^{(1)}a_2\right), \tag{A.13}$$

$$F_{13} = \frac{a_2a_3 - a_1a_4 + \left(1 + e^{-2|\alpha_1|h_1}\right)\left(1 - e^{-4|\alpha_1|h_1}\right)\left[\left(e_{15}^{(1)} + \varepsilon_{11}^{(1)}\right)a_1 - \left(c_{44}^{(1)} + e_{15}^{(1)}\right)a_2\right]}{\left(1 + e^{-2|\alpha_1|h_1}\right)}, \tag{A.14}$$

$$F_{14} = \frac{\left(1 + e^{-2|\alpha_1|h_1}\right)\left(1 - e^{-4|\alpha_1|h_1}\right)\left[\left(e_{15}^{(1)} + \varepsilon_{11}^{(1)}\right)a_1 - e_{15}^{(1)}a_2\right]}{\left(1 + e^{-2|\alpha_1|h_1}\right)}, \tag{A.15}$$

$$F_{15} = e^{-2|\alpha_2|h_2}\left(1 - e^{-4|\alpha_1|h_1}\right)\left[\left(e_{15}^{(1)} + \varepsilon_{11}^{(1)}\right)a_1 - \left(c_{44}^{(1)} + e_{15}^{(1)}\right)a_2\right], \tag{A.16}$$

$$F_{16} = e^{-2|\alpha_2|h_2}\left(1 - e^{-4|\alpha_1|h_1}\right)\left[\left(e_{15}^{(1)} + \varepsilon_{11}^{(1)}\right)a_1 - e_{15}^{(1)}a_2\right], \tag{A.17}$$

where

$$a_1 = \left(1 - e^{-2|\alpha_2|h_2}\right)\left(1 + e^{-2|\alpha_1|h_1}\right)\left(c_{44}^{(2)} + e_{15}^{(2)}\right) - \left(1 - e^{-2|\alpha_1|h_1}\right)\left(1 + e^{-2|\alpha_2|h_2}\right)\left(c_{44}^{(1)} + e_{15}^{(1)}\right), \tag{A.18}$$

$$a_2 = \left(1 - e^{-2|\alpha_2|h_2}\right)\left(1 + e^{-2|\alpha_1|h_1}\right)e_{15}^{(2)} - \left(1 - e^{-2|\alpha_1|h_1}\right)\left(1 + e^{-2|\alpha_2|h_2}\right)e_{15}^{(1)}, \tag{A.19}$$

$$a_3 = \left(1 - e^{-2|\alpha_2|h_2}\right)\left(1 + e^{-2|\alpha|h_1}\right)\varepsilon_{11}^{(2)} + \left(1 - e^{-2|\alpha|h_1}\right)\left(1 + e^{-2|\alpha|h_2}\right)\varepsilon_{11}^{(1)}, \tag{A.20}$$

$$a_4 = -\left(1 - e^{-2|\alpha_2|h_2}\right)\left(1 + e^{-2|\alpha_1|h_1}\right)\left(e_{15}^{(2)} + \varepsilon_{11}^{(2)}\right) + \left(1 - e^{-2|\alpha|h_1}\right)\left(1 + e^{-2|\alpha|h_2}\right)\left(e_{15}^{(1)} + \varepsilon_{11}^{(1)}\right), \tag{A.21}$$

B. The Structural Expression of First Kind of Cauchy Singular Integral Equations

The expressions in equations (59) and (60) are as follows:

$$\begin{aligned} Q_{1*} = {} & \left(c_{44}^{(2)} + e_{15}^{(2)}\right)\left[\left(c_{44}^{(1)} + e_{15}^{(1)}\right)\left(\varepsilon_{11}^{(2)} - \varepsilon_{11}^{(1)}\right) - e_{15}^{(1)}\left(e_{15}^{(2)} - e_{15}^{(1)}\right)\right] \\ & + e_{15}^{(2)}\left[\left(\left(e_{15}^{(1)} + \varepsilon_{11}^{(1)}\right)\left(c_{44}^{(2)} - c_{44}^{(1)} + e_{15}^{(2)} - e_{15}^{(1)}\right) - \left(c_{44}^{(2)} + e_{15}^{(2)}\right)\left(e_{15}^{(2)} - e_{15}^{(1)}\right)\right)\right], \end{aligned} \tag{B.1}$$

$$Q_{2*} = \left(c_{44}^{(2)} + e_{15}^{(2)}\right)\left[\left(e_{15}^{(2)} + \varepsilon_{11}^{(2)}\right)\left(e_{15}^{(2)} - e_{15}^{(1)} + \varepsilon_{11}^{(2)} - \varepsilon_{11}^{(1)}\right) - \varepsilon_{11}^{(1)}\left(\varepsilon_{11}^{(2)} - \varepsilon_{11}^{(1)}\right)\right] + e_{15}^{(2)}\left[\left(e_{15}^{(1)} + \varepsilon_{11}^{(1)}\right)\left(c_{44}^{(2)} - c_{44}^{(1)} + e_{15}^{(2)} - e_{15}^{(1)}\right) - e_{15}^{(1)}\left(e_{15}^{(2)} - e_{15}^{(1)}\right)\right], \tag{B.2}$$

$$Q_{3*} = \left(e_{15}^{(2)} + \varepsilon_{11}^{(2)}\right)\left[\left(c_{44}^{(1)} + e_{15}^{(1)}\right)\left(\varepsilon_{11}^{(2)} - \varepsilon_{11}^{(1)}\right) - e_{15}^{(1)}\left(e_{15}^{(2)} - e_{15}^{(1)}\right)\right] + \varepsilon_{11}^{(2)}\left[\left(\left(e_{15}^{(1)} + \varepsilon_{11}^{(1)}\right)\left(c_{44}^{(2)} - c_{44}^{(1)} + e_{15}^{(2)} - e_{15}^{(1)}\right) - \left(c_{44}^{(2)} + e_{15}^{(2)}\right)\left(e_{15}^{(2)} - e_{15}^{(1)}\right)\right)\right], \tag{B.3}$$

$$x \qquad Q_{4*} = \left(e_{15}^{(2)} + \varepsilon_{11}^{(2)}\right)\left[\left(e_{15}^{(2)} + \varepsilon_{11}^{(2)}\right)\left(e_{15}^{(2)} - e_{15}^{(1)} + \varepsilon_{11}^{(2)} - \varepsilon_{11}^{(1)}\right) - \varepsilon_{11}^{(1)}\left(\varepsilon_{11}^{(2)} - \varepsilon_{11}^{(1)}\right)\right] + \varepsilon_{11}^{(2)}\left[\left(e_{15}^{(1)} + \varepsilon_{11}^{(1)}\right)\left(c_{44}^{(2)} - c_{44}^{(1)} + e_{15}^{(2)} - e_{15}^{(1)}\right) - e_{15}^{(1)}\left(e_{15}^{(2)} - e_{15}^{(1)}\right)\right], \tag{B.4}$$

$$F_* = \left(e_{15}^{(2)} - e_{15}^{(1)}\right)\left(\varepsilon_{11}^{(2)} - \varepsilon_{11}^{(1)}\right) - \left(c_{44}^{(2)} - c_{44}^{(1)} + e_{15}^{(2)} - e_{15}^{(1)}\right)\left(e_{15}^{(2)} - e_{15}^{(1)} + \varepsilon_{11}^{(2)} - \varepsilon_{11}^{(1)}\right), \tag{B.5}$$

$$k_1(x,t,\omega) = \int_0^\infty \left(\frac{Q_1(s,\omega)}{F} - \frac{Q_{1*}}{F_*}\right)\sin(s(t-x))ds,$$

$$k_2(x,t,\omega) = \int_0^\infty \left(\frac{Q_2(s,\omega)}{F} - \frac{Q_{2*}}{F_*}\right)\sin(s(t-x))ds, \tag{B.6}$$

$$k_3(x,t,\omega) = \int_0^\infty \left(\frac{Q_3(s,\omega)}{F} - \frac{Q_{3*}}{F_*}\right)\sin(s(t-x))ds, \tag{B.7}$$

$$k_4(x,t,\omega) = \int_0^\infty \left(\frac{Q_4(s,\omega)}{F} - \frac{Q_{4*}}{F_*}\right)\sin(s(t-x))ds. \tag{B.8}$$

(B.9)

C. Elements in Dislocation Density Function

The expressions in equations (66) and (67) are as follows:

$$r_j = \frac{x_j - c_{0j}}{a_{0j}},\ s_j = \frac{t_j - c_{0j}}{a_{0j}}, \tag{C.1}$$

$$g_W^{*(j)}(x,\omega) = f_1^{(j)}(x,\omega),\ g_\Phi^{*(j)}(x,\omega) = f_2^{(j)}(x,\omega), \tag{C.2}$$

$$k_i(x,t,\omega) = L_i(r,s,\omega)\ \ (i = 1,2,3,4), \tag{C.3}$$

$$a_{0j} = \frac{b_j - a_j}{2},\ c_{0j} = \frac{b_j + a_j}{2},\ \ (j = 1,2,\ldots,n). \tag{C.4}$$

Data Availability

All the numerical calculated data used to support the findings of this study can be obtained by calculating the equations in the paper, and piezoelectric material parameters are taken from existing references.

Conflicts of Interest

The authors declare that there are no conflicts of interest regarding the publication of this paper.

Acknowledgments

This study was funded by the Startup Project of Doctor Scientific Research of Zhoukou Normal University (ZKNUC2021004).

References

[1] Y. E. Pak, "Crack extension force in a piezoelectric material," *Journal of Applied Mechanics*, vol. 57, no. 3, pp. 647–653, 1990.

[2] A. K. Soh, D.-N. Fang, and K. L. Lee, "Analysis of a bi-piezoelectric ceramic layer with an interfacial crack subjected to anti-plane shear and in-plane electric loading," *European Journal of Mechanics - A/Solids*, vol. 19, no. 6, pp. 961–977, 2000.

[3] H. G. Beom and S. N. Atluri, "Near-tip fields and intensity factors for interfacial cracks in dissimilar anisotropic piezoelectric media," *International Journal of Fracture*, vol. 75, pp. 163–183, 1996.

[4] Z. T. Chen and M. J. Worswick, "Antiplane mechanical and inplane electric time-dependent load applied to two coplanar cracks in piezoelectric ceramic material," *Theoretical and Applied Fracture Mechanics*, vol. 33, no. 3, pp. 173–184, 2000.

[5] X. Wang, Z. Zhong, and F. L. Wu, "A moving conducting crack at the interface of two dissimilar piezoelectric materials," *International Journal of Solids and Structures*, vol. 40, no. 10, pp. 2381–2399, 2003.

[6] X.-F. Li and G. J. Tang, "Antiplane interface crack between two bonded dissimilar piezoelectric layers," *European Journal of Mechanics - A/Solids*, vol. 22, no. 2, pp. 231–242, 2003.

[7] X. Wang and S. Yu, "Transient response of a crack in piezoelectric strip subjected to the mechanical and electrical impacts: mode-III problem," *International Journal of Solids and Structures*, vol. 37, no. 40, pp. 5795–5808, 2000.

[8] B. Gu, X. Wang, S. Yu, and D. Gross, "Transient response of a Griffith crack between dissimilar piezoelectric layers under anti-plane mechanical and in-plane electrical impacts," *Engineering Fracture Mechanics*, vol. 69, no. 5, pp. 565–576, 2002.

[9] X.-C. Zhong, F. Liu, and X.-F. Li, "Transient response of a magnetoelectroelastic solid with two collinear dielectric cracks under impacts," *International Journal of Solids and Structures*, vol. 46, no. 14-15, pp. 2950–2958, 2009.

[10] F. Liu and X.-C. Zhong, "Transient response of two collinear dielectric cracks in a piezoelectric solid under inplane impacts," *Applied Mathematics and Computation*, vol. 217, no. 8, pp. 3779–3791, 2010.

[11] J. Aboudi, "Transient response of piezoelectric composites caused by the sudden formation of localized defects," *International Journal of Solids and Structures*, vol. 50, no. 16-17, pp. 2641–2658, 2013.

[12] J. W. Shin and T.-U. Kim, "Transient response of a Mode III interface crack between piezoelectric layer and functionally graded orthotropic layer," *International Journal of Solids and Structures*, vol. 90, pp. 122–128, 2016.

[13] A. H. Fartash, M. Ayatollahi, and R. Bagheri, "Transient response of dissimilar piezoelectric layers with multiple interacting interface cracks," *Applied Mathematical Modelling*, vol. 66, pp. 508–526, 2019.

[14] R. Wang, E. Tang, G. Yang, Y. Han, and C. Chen, "Dynamic fracture behavior of piezoelectric ceramics under impact: force-electric response and electrical breakdown," *Journal of The European Ceramic Society*, vol. 41, no. 16, pp. 139–150, 2021.

[15] J. W. Shin, Y.-S. Lee, and S. J. Kim, "Transient response of a crack in a functionally graded piezoelectric strip between two dissimilar piezoelectric strips," *Theoretical and Applied Fracture Mechanics*, vol. 66, pp. 9–15, 2013.

[16] R. Bagheri, "Several horizontal cracks in a piezoelectric half-plane under transient loading," *Archive of Applied Mechanics*, vol. 87, pp. 1979–1992, 2017.

[17] H. Ershad, R. Bagheri, and M. Noroozi, "Transient response of cracked nonhomogeneous substrate with piezoelectric coating by dislocation method," *Mathematics and Mechanics of Solids*, vol. 23, no. 12, pp. 1525–1536, 2018.

[18] A. G. Milan and M. Ayatollahi, "Transient analysis of multiple interface cracks between two dissimilar functionally graded magneto-electro-elastic layers," *Archive of Applied Mechanics*, vol. 90, pp. 1829–1844, 2020.

[19] W. Yang, M. Nourazar, Z. Chen, K. Hu, and X. Zhang, "Dynamic response of a cracked thermopiezoelectric strip under thermo-electric loading using fractional heat conduction," *Applied Mathematical Modelling*, vol. 103, pp. 580–603, 2022.

[20] S. Hu, J. Liu, J. Li, and X. Xie, "Interaction of screw dislocation with edge interfacial crack on fine-grained piezoelectric coating/substrate," *Advances in Materials Science and Engineering*, vol. 2019, Article ID 3848240, 13 pages, 2019.

[21] S. Hu, J. Liu, and J. Li, "Research on multiple griffith cracks at the interface of fine-grained piezoelectric coating/substrate," *Mathematical Problems in Engineering*, vol. 2019, Article ID 2547891, 14 pages, 2019.

[22] S. Hu, J. Liu, and J. Li, "Fracture analysis of griffith interface crack in fine-grained piezoelectric coating/substrate under thermal loading," *Advances in Mathematical Physics*, vol. 2020, Article ID 4201591, 15 pages, 2020.

[23] A. J. Bell and A. J. Moulson, "The effect of grain size on the dielectric properties of barium titanate ceramic," *Journal of The American Ceramic Society*, vol. 62, pp. 325–328, 1985.

[24] R. P. S. M. Lobo, N. D. S. Mohallem, and R. L. Moreira, "Grain-size effects on diffuse phase transitions of sol-gel prepared barium titanate ceramics," *Journal of The American Ceramic Society*, vol. 78, no. 5, pp. 1343–1346, 1995.

[25] F. Erdogan, G. D. Gupta, and T. S. Cook, "Numerical solution of singular integral equations," in *Methods of Analysis and Solutions of Crack Problems*, G. C. Sih, Ed., pp. 368–425, Springer, Dordrecht, Noordhoff, Leyden, The Netherlands, 1973.